Asymmetry and bifurcations in three-dimensional sudden-contraction channel flows

T. P. Chiang,[1] Amalendu Sau,[2,*] and Robert R. Hwang[3]
[1]*Department of Engineering Sciences and Ocean Engineering, National Taiwan University, Taipei, Taiwan*
[2]*Department of Mechanical and Aerospace Engineering, Gyeongsang National University, Jinju, South Korea*
[3]*Institute of Physics, Academia Sinica, Taipei, Taiwan*

(Received 8 November 2010; revised manuscript received 21 February 2011; published 22 April 2011)

This study reports the presence of two different stable modes of bifurcation in the near field of a three-dimensional sudden contraction. To be precise, flow downstream of a symmetric sudden contraction undergoes a transition from a symmetric state to an asymmetric state through a symmetry-breaking pitchfork bifurcation following an increase in the channel aspect ratio or the Reynolds number. In addition, the oncoming (upstream) symmetry-plane flow exhibits spanwise bifurcations along the topological core lines of each of the salient roof and floor eddies. Small aspect-ratio (contraction) channels are noted to facilitate interesting splitting of the salient roof and floor eddies into multicore forms with accompanying spanwise flow bifurcations along the respective vortical core lines. Herein extensive three-dimensional simulations performed with various aspect and contraction ratios and Reynolds numbers clearly suggest that flow transition in the sudden-contraction channels should indeed occur primarily through these two generically distinct modes of bifurcation.

DOI: 10.1103/PhysRevE.83.046313 PACS number(s): 47.10.ad, 47.11.Df, 47.15.Rq, 47.20.Ky

I. INTRODUCTION

Flow through a contraction channel with steps is one of the simplest models that is inhomogeneous in the flow direction, and appears to display interesting pitchfork bifurcating solutions at higher aspect ratios. On the other hand, such entry flow problems are of fundamental interest in understanding kinematics of viscoelastic flows (melt flow instability), in particular, in polymer processing. However, unlike for flows in channels with a suddenly expanded part, the exploration of flow physics around three-dimensional sudden contractions is yet to receive adequate attention. An early review covering both Newtonian and non-Newtonian aspects of flows around sudden contraction is provided by Boger [1]. In general, the important physically distinguishable flow features around the contraction area (Fig. 1) may be characterized as (i) the formation of two recirculating eddies at the upstream *salient corners* and (ii) the growth of two separation bubbles (*tip corner eddies*) immediately downstream of the plane of contraction. Notably, while most of the available investigations (e.g., Dennis and Smith [2], Durst and Loy [3], Durst *et al.* [4], Hawken *et al.* [5], and Huang and Seymour [6]) on the topic remained concerned with two-dimensional (2D) flow behaviors observed at moderate Reynolds numbers, almost all practical flow situations are, however, inherently three dimensional and they often occur at a relatively higher Reynolds number (Re). Notably, in three dimensions the physically sensitive critical parameters in a sudden-contraction flow are the aspect ratio A, the contraction ratio C, and the Re. According to Dennis and Smith [2], for a fixed contraction ratio $C = 2$ (and $\mathrm{Re} < 1000$), the separation length L_1 of the upstream salient eddy (comprising a single recirculating bubble, as shown in Fig. 1) varies linearly with Re, i.e., $L_1 = 0.1289\ln(\mathrm{Re}) - 0.547$. Furthermore, existing (two-dimensional) investigations report symmetrical growth of single-core upstream separation bubbles (with the same separation lengths L_1 extending along the channel roof and floor and the same reattachment lengths L_2 over the two vertical planes of contraction) along the roof and floor of the channel (Fig. 1). However, our three-dimensional (3D) simulations in setups having relatively lower aspect ratios demonstrate interesting near-transitional splitting behavior of the salient roof and floor eddies (formed immediately upstream of the plane of contraction). In addition, the presently observed phenomenon of the occurrence of spanwise flow bifurcations along critical core lines of (split) salient roof and floor eddies remained virtually unknown. Moreover, we note the clear persistence of pitchfork bifurcation in the downstream flow beyond a critical Reynolds number. One of the aims of the present study is therefore to explore these physically sensitive important (but relatively unknown) flow phenomena in three dimensions (which are noted to occur in the vicinity of two steps of the sudden contraction) and extract the governing physics.

Notably, over the years, the transition behavior of flows in symmetric sudden-expansion channels has been investigated extensively. To this point, experimental findings of Durst *et al.* [7] and Cherdron *et al.* [8] demonstrate that such expansion flows (in a perfectly symmetric setup) remain symmetric at low Reynolds numbers, but become asymmetric at a higher Re. Later, Fearn *et al.* [9] found that the asymmetry in the flow above some critical Re appears due to a pitchfork bifurcation. On the other hand, Mizushima *et al.* [10] numerically investigated the stability of two-dimensional flows in a symmetric channel with a suddenly expanded and contracted part. According to their findings, the flow in the setup remains steady and symmetric at low Reynolds numbers, becomes asymmetric at a critical Reynolds number Re_1 due to symmetry-breaking pitchfork bifurcation, and regains symmetry at another critical Reynolds number Re_2 owing to another pitchfork bifurcation. The symmetric flow eventually becomes oscillatory at some other critical Reynolds number Re_3 owing to a Hopf bifurcation. Remarkably, the aspect ratio of such an expansion-contraction channel was

*Corresponding author: amalendu.sau@gmail.com

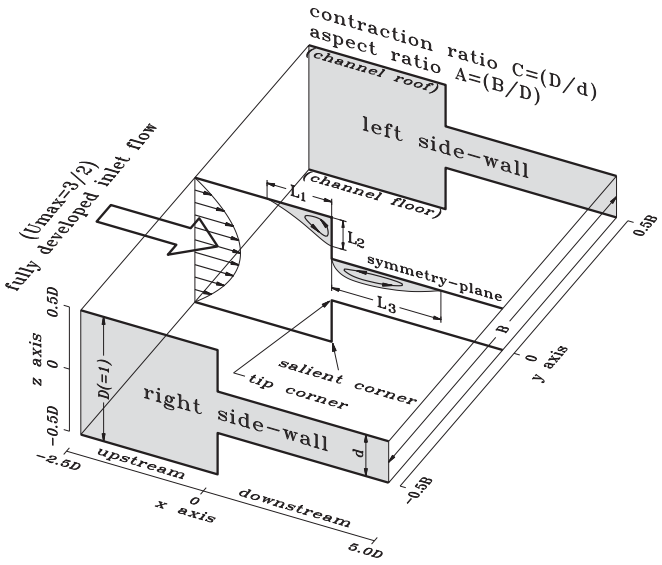

FIG. 1. Schematic of the three-dimensional contraction channel flow and its symmetry-plane features.

found to have a profound effect on the unstable growth of the downstream flow. An exchange of modes with oscillatory instabilities was found to occur for the flow as the aspect ratio, the ratio of the length of the expanded part to its width, varied. For the channel aspect ratio 2.44, hysteresis was noted to occur (Ref. [11]) for a certain range of Reynolds numbers, in which the setup facilitates the growth of two stable and two unstable asymmetric solutions and a stable symmetric solution. In contrary, it is interesting to note that the corresponding three-dimensional flows [12] exhibit perfectly symmetric solutions, with no sign of bifurcation.

On the other hand, surprisingly, the present investigation concerning three-dimensional flow evolution in a symmetric sudden contraction channel reveals the coexistence of two different modes of dominant bifurcating solutions in the setup, and such flow bifurcations in 3D remained virtually unexplored. Notably, most of the existing investigations (e.g., Refs. [2,4–6]) preassumed the symmetric nature of the flow and often conducted 2D simulations in the half-channel. However, our simulated results, covering a wide range of physically sensitive parameter spaces, clearly indicate that the pitchfork bifurcation remains inherently the strongest feature of 3D plane sudden-contraction channel flows. In addition, a physically significant new phenomenon is noted to occur in these three-dimensional contraction flows, that is, the occurrence of spanwise bifurcation of the oncoming upstream symmetry-plane flow along each of the topological core lines of salient roof and floor eddies. While being consistent, in the present study we aim to exploit these important bifurcation characteristics of 3D sudden-contraction channel flows, and extract the unknown inner physics.

II. MATHEMATICAL MODEL AND THE NUMERICAL IMPLEMENTATION

The physical problem considered here is the three-dimensional steady incompressible flow evolution through a planner symmetric channel with sudden contraction. Fully developed laminar flow enters into the channel inlet situated at a streamwise distance $2.5D$ upstream of the plane of contraction (D being the transverse width of the inlet channel), and the length of the contraction part is $5D$ ($\equiv 20\,d$ or $10\,d$, depending on the contraction ratio; d is the width of the symmetric channel downstream of the plane of contraction). Therefore, the two equal sized step heights of the channel became $(D-d)/2$, leading to channel contraction ratio $C = D/d$. Notably, our flow configuration remained consistent with the past experimental [4] and computational [5,6] setups used for corresponding two-dimensional investigations. In order to have a broader understanding of the developed flow and to clearly establish the governing physics (including different bifurcation scenarios), the spanwise width "B" ($B = AD$, A being the aspect ratio) of the channel was carefully varied between $0.5D$ and $48D$. In a rectangular Cartesian coordinate system with the origin situated at the center of the plane of contraction (Fig. 1), the x axis (which coincides with the channel axis) is taken along the streamwise direction, the y axis remained directed along the channel span, and the z axis is taken along the step height. Extensive 3D flow simulations in the setup are carefully conducted with five different Reynolds numbers, 1250, 1500, 1750, 3150, and 3500, two different contraction ratios, $C = 2$ and $C = 4$, and a sequence of 26 values of channel aspect ratio within $0.5D \leqslant A \leqslant 48D$, to clearly establish the associated physics.

The flow characteristics in the physical setup are modeled by the three-dimensional steady incompressible Navier-Stokes equations,

$$\underline{u} \cdot \nabla \underline{u} = -\nabla p + \nabla^2 \underline{u}/\mathrm{Re}, \tag{1}$$

$$\nabla \cdot \underline{u} = 0, \tag{2}$$

where all lengths have been nondimensionalized by the transverse channel width D ($\equiv 1$) upstream of contraction. The velocities are normalized with respect to the chosen characteristic velocity U_{ch}, which takes on a value 2/3 times that of the inlet maximum velocity $u_{\max}$ ($\equiv 3/2$), and the pressure is nondimensionalized with respect to ρU_{ch}^2. The Reynolds number of the flow is defined as

$$\mathrm{Re} = \left[(2/3)u_{\max}\right]D/V.$$

Concerning the implemented boundary conditions, for all the investigated cases we specify fully developed velocity profiles (e.g., see Ref. [13]) at the channel inlet, and at the exit a zero gradient outflow boundary condition is used. Along the sidewalls no-slip conditions are specified. Notably, with the help of presently adopted primitive variable formulations we carefully avoided the undesirable scenario of encountering corner singularities (of infinite vorticity at the tip corners) that were often faced (e.g., Refs. [2,6]) while using the stream-function vorticity approach.

In order to calculate the velocity ($\underline{u}$) and pressure (p) fields numerically, the primitive-variable equations (1) and (2) have been discretized using a well-refined staggered multigrid (control volume) system of 2.97×10^6 nodes of variable

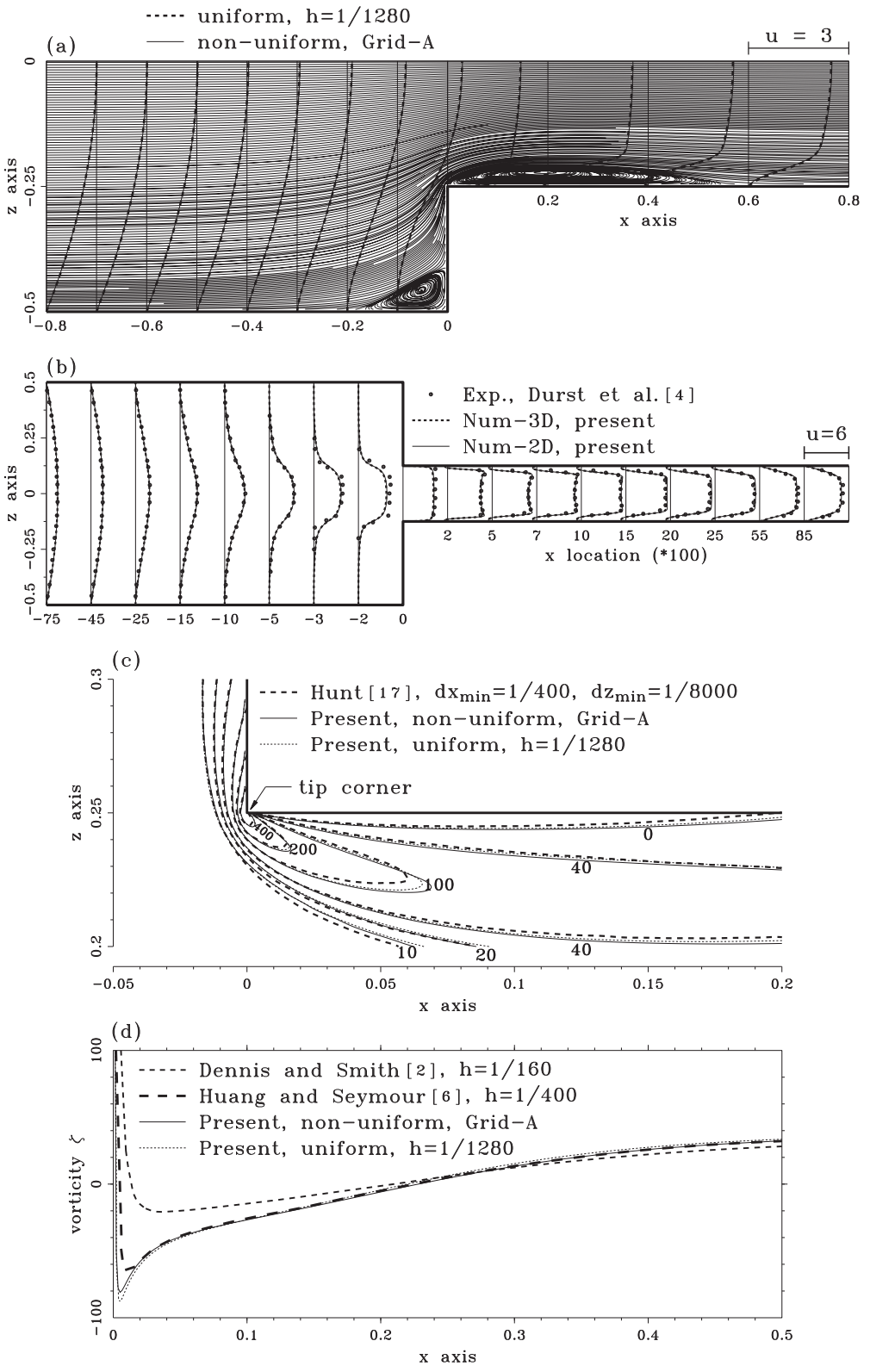

FIG. 2. Comparison of present results with those obtained using various uniform/nonuniform grids and symmetry-plane (2D) measurements for the contraction flows. (a) Streamwise velocity (u) profiles (on $y = 0$) through different stations, Re $= 2000$, $C = 2$; (b) computed two- and three-dimensional u-velocity profiles on the plane of symmetry $y = 0$ and the experimental prediction of Durst *et al.* [4], Re $= 1150$, $C = 4$; (c) comparison of presently simulated vorticity field with those obtained by using the stream-function-vorticity approach, Re $= 1000$, $C = 2$; and (d) vorticity along downstream channel roof/floor, $C = 2$, Re $= 1000$. h is the uniform grid width.

width. The convective terms in the momentum equations are discretized by a modified version of the third order accurate Quick scheme of Leonard [14], which accommodates suitable distributions of nonuniform grids (see Ref. [15] for details).

TABLE I. Details of the nonuniform grid-A.

C	x(min, max)	$N(dx,dy,dz)$	dx(min,max)	dy(min,max)	dz(min,max)
2	(−2.5, 5.0)	(110, 150, 160)	(0.001, 0.25)	(0.01, 0.24)	(0.001, 0.02)
4	(−2.5, 5.0)	(110, 150, 180)	(0.001, 0.25)	(0.01, 0.24)	(0.001, 0.01)

This appeared necessary in order to accurately resolve the local growth of vortical structures particularly near the sharp edges/corners. The viscous terms are discretized using a second order accurate central difference scheme. As far as a solution algorithm is concerned, we adopted the Simple-C method of Van Doormaal and Raithby [16] to achieve accurate results at a faster convergence rate. The pressure field is solved using the pressure-velocity coupling method. Notably, for all the investigated cases, the solution was considered to have converged when global L_2 norms of pressure and velocity residuals reached a value below 10^{-12}. The solver was thoroughly validated, first by taking into account the grid independence of the computed results, and second by obtaining a good comparison of our simulated results with the previous relevant investigations. The optimized nonuniform grid length scales with finer grids placed near the sharp corner/reverse-flow regions are presented in Table I. On the other hand, it is noteworthy that Fig. 2 clearly demonstrates that our simulated results obtained with both uniform and nonuniform grids compare quite well with those of Durst *et al.* [4], Hunt [17], Dennis and Smith [2], and Huang and Seymour [6].

III. RESULTS AND DISCUSSION

Notably, the primary objective of the present investigation is to provide an in-depth understanding of the observed bifurcating flow behavior in the near field of a 3D plane symmetric sudden contraction. However, for the sake of consistency, we begin the section by presenting some of the simulated two-dimensional flow features. Figure 3(a) illustrates the detailed symmetry-plane ($y = 0$) characteristics of the developed nonbifurcating steady flow (in a channel having contraction ratio $C = 4$ and aspect ratio $A = 4$) in association with superimposed streamwise (u) velocity profiles through different stations. First, our simulated flow characteristics (and u-velocity profiles) at this relatively lower Reynolds number (Re = 1500) and moderate channel aspect ratio ($A = 4$) remained quite consistent with the experimental findings of Durst and Loy [3]. Second, an important thing to note here is the perfect axially symmetric growth of the simulated flow in association with two pairs of equal sized roof and floor eddies [Fig. 3(a)] located at the upstream salient corners and downstream *tip corners*. Note particularly that at this moderate aspect ratio the developed roof (salient/tip) eddies and their floor counterparts have the same separation/reattachment lengths L_1, L_2, and L_3 (Fig. 1).

Figure 3(b) presents the near-critical flow behavior in a significantly high aspect-ratio ($A = 24$) channel that facilitates the onset of asymmetry/bifurcation (in a perfectly symmetric setup). Remarkably, it displays unequal/asymmetrical structural growth of two tip corner eddies (behind the plane of contraction), with the floor eddy appearing significantly (two times) larger than the corresponding roof tip eddy. Such an asymmetric flow development (in a perfectly symmetric

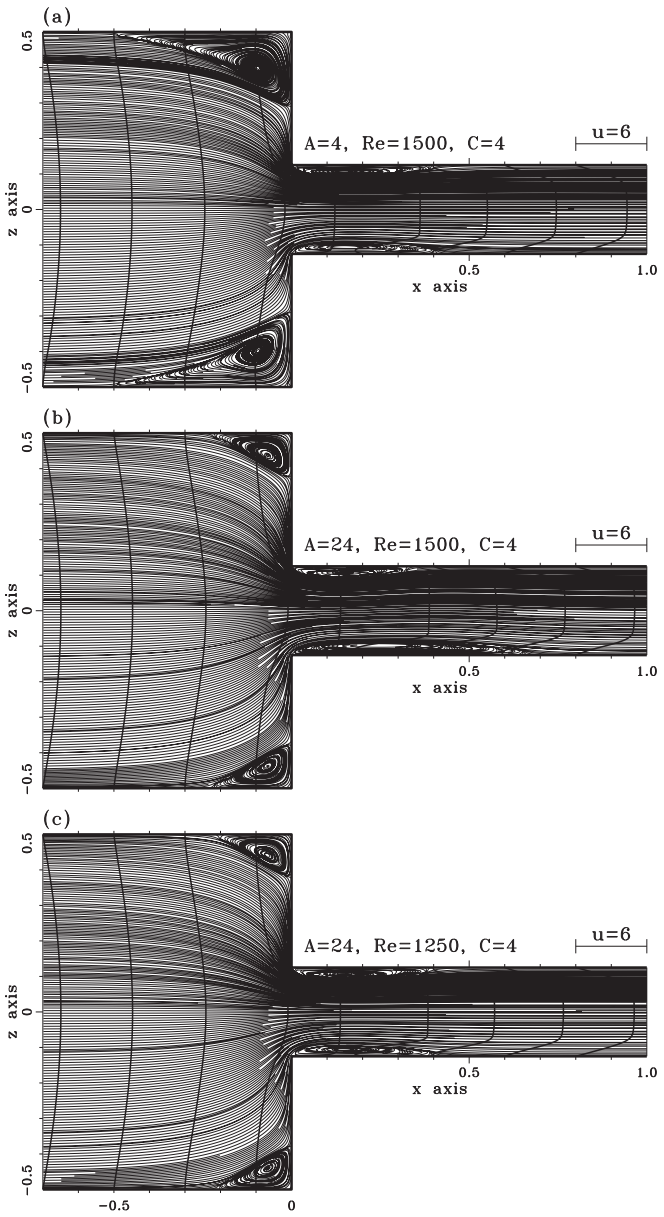

FIG. 3. Streamwise flow development in a channel with contraction ratio $C = 4$. (a) Perfectly symmetrical structural growths of streamlines on $y = 0$ and u-velocity profiles through different streamwise stations reveal the typical nonbifurcating flow behavior in the setup. (b) Symmetry-plane flow features with $A = 24$ reveal unequal growth of tip eddies over the channel roof and floor, and the onset of pitchfork bifurcation. (c) Restoration of nonbifurcating flow in the setup at Re = 1250, $A = 24$.

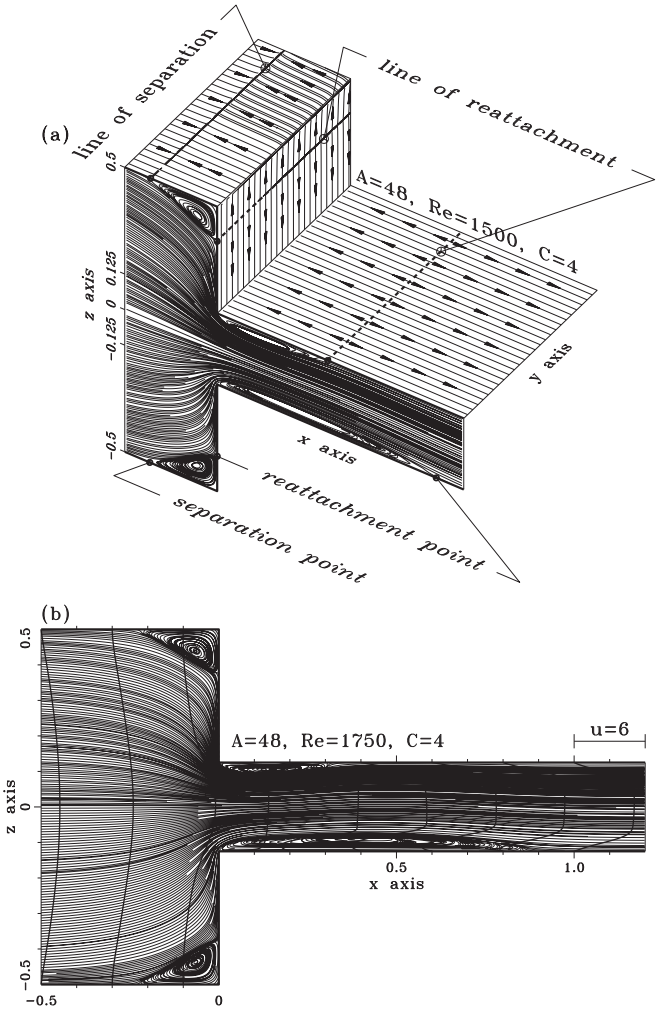

FIG. 4. Persistence of pitchfork bifurcating solutions with enhanced asymmetry in a contraction channel having high aspect ratio. (a) Streamlines (on $y = 0$) and extracted u-velocity profiles at $A = 48$. (b) Continuation of pitchfork bifurcation at a higher Reynolds number, Re $= 1750$.

contraction channel), which signals physical flow transition from a predominantly symmetric [Fig. 3(a)] state to a visibly asymmetric [Fig. 3(b)] state (just behind the plane of contraction), occurring due to pitchfork bifurcation. Note that for the bifurcating flow the reattachment length $L_{3,\text{roof}}$ (as schematically shown in Fig. 1) along the channel roof became significantly shorter than the corresponding floor reattachment length $L_{3,\text{floor}}$. Furthermore, readers may carefully note here [Figs. 3(b) and 4] the initiation of the asymmetric appearance of u-velocity profiles with respect to the channel axis (for $x \geqslant 0.4$). Interestingly, unlike downstream (roof and floor) reattachment lengths (L_3), the separation length L_1 and the reattachment length L_2 (as defined in Fig. 1) of the two salient (roof and floor) eddies [Fig. 3(b)] remained exactly the same. Therefore, the observed distinctive characteristic of pitchfork bifurcation of high aspect-ratio flows remains exclusively dependent on unequal growth of the (roof and floor) tip corner eddies. Note, however, that at a relatively lower Reynolds number Re $= 1250$ (but with the same aspect ratio $\boldsymbol{A} = 24$, and the same contraction ratio $C = 4$) the flow recovered a visibly symmetric state again [Fig. 3(c)], comprising equal sized tip (and salient) eddies on the channel floor and roof. This clearly suggests the existence of a critical Re (for a fixed set of physical parameters) beyond which the contraction flow continues to exhibit pitchfork bifurcation. Importantly, the phenomenon of growth of unequal/asymmetric separation zones in channels with a sudden expansion part has been attributed to instability of the wall shear layer [7,8], although the phenomenon has been termed the "*Coanda effect*." The origin of such (steady) asymmetric streamwise flows in a symmetric sudden-expansion channel is verified [9,18] to be the pitchfork bifurcation. Notably, we observe here a similar symmetry-breaking bifurcation to persist in the flow downstream of a three-dimensional sudden contraction. In addition, note [Figs. 3(a) and 3(b)] the considerable shrinkage of separation length L_1 (streamwise elongation of the salient eddy, as sketched in Fig. 1) with the increase of aspect ratio A. For the sake of further clarity, Fig. 4 exhibits the persistence of pitchfork bifurcations in the contraction channel flows not only with a larger aspect ratio [$A = 48$, Fig. 4(a)], but also at a higher Reynolds number [Re $= 1750$, Fig. 4(b)]. These lengthy but careful simulations with a number of values of aspect ratio (A) are particularly conducted to ensure that the bifurcations are not really end-wall induced. In contrary, as it turns out, the wider we take the channel span (aspect ratio), the easier it becomes to maintain a sustainable bifurcating solution. We now also make it clear that the longer reattachment length (L_3) can form randomly either on the floor or along the roof of the symmetric channel with equal probabilities, although direction biasness here is determined presumably by the algorithm used in the computation [18]. Importantly, however, the demonstrated findings [Fig. 4(b)] at Re $= 1750$ (and high Reynolds number flows presented later) seem to suggest that the onset of flow transition in sudden contraction channels must occur in association with a pitchfork bifurcation. We would also like to state here that, while the critical flow features (e.g., Figs. 3 and 4) are being presented for the near field of the plane of contraction (the actual upstream channel length is at least five times larger, and the downstream length is twenty times larger), extensive experimentation has been done to ensure that the inlet and the exit locations/conditions have no influence on the internal vortical flow development.

Notably, the critical value of Re (leading to pitchfork bifurcation) in a setup depends both on the aspect ratio (A) and the contraction ratio (C). However, extracting such a critical Re from the lengthy 3D simulations seems to appear an unfeasible task. On the other hand, based on our recent 2D computations [19], the estimates (Fig. 5) of critical Reynolds numbers for channels with contraction ratios $C = 2$ and $C = 4$ are evaluated as 3080 and 1350, respectively. On the basis of experience gained from these reference 2D solutions, we conducted a series of 3D simulations in the full domain with various channel aspect ratios ($0.5 \leqslant A \leqslant 48$) to confirm that the observed pitchfork bifurcation is indeed an inseparable physical characteristic of the sudden contraction channel flows; and subsequently, we explored possibilities of coexistence of other spanwise bifurcating type [20] solutions in the setup. For the sake of improved reliability/clarity the sequential variation of separation/attachment lengths L_1, L_2, and L_3, with A of

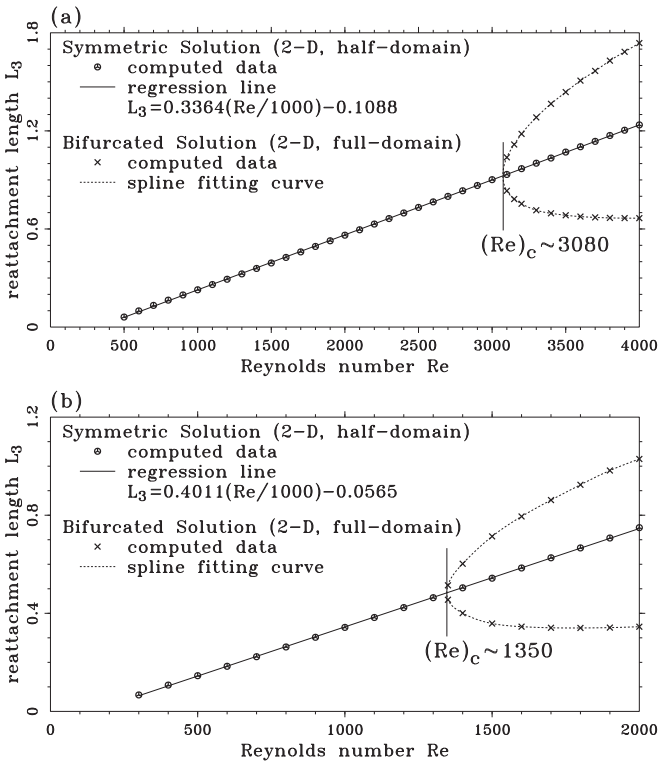

FIG. 5. Bifurcation diagram obtained from the simulated reattachment lengths L_3 of the downstream tip eddy. (a) $C = 2$ and (b) $C = 4$.

the developed salient/tip eddies corresponding to (C, Re) = (4, 1500) are extracted in Table II along with the 2D reference value. It clearly shows a consistent sharp increase of $L_{3,\text{floor}}$ over $L_{3,\text{roof}}$ (of the tip eddies) for channels having aspect ratios $A \geqslant 5$, signifying the onset of pitchfork bifurcation in sudden-contraction flows.

In an effort to unfold detailed three-dimensional physical evolution characteristics of the flow in association with observed salient/tip eddies and to investigate the unknown physics, in Fig. 6 we extract critical flow dynamics surrounding the topologically important core lines of the various vortices. The vortex core lines A_iB_i (e.g., thick lines in Fig. 6) for the investigated various cases (see also Ref. [21]) are computed based on the velocity gradient eigenmode method, namely, the λ_2 definition of Jeong and Hussain [22], and they seem to carry much of the inner flow physics. Notably, in the λ_2 method the velocity gradient tensor $\nabla \underline{u}$ is decomposed into its symmetric part, the rate of deformation or strain tensor $\mathbf{S}$, and its antisymmetric part, the spin tensor Ω. Then three eigenvalues λ_1, λ_2, and λ_3 of the tensor $\mathbf{M} = \mathbf{S}^2 + \Omega^2$ are determined and ordered such that $\lambda_1 \leqslant \lambda_2 \leqslant \lambda_3$. Note that $\mathbf{M}$ has only real eigenvalues, since it is symmetric. According to the λ_2 definition [22], a vortex is a region in space for which the matrix $\mathbf{M}$ has two negative eigenvalues. The surface of the vortex is defined by the set of points for which $\lambda_1 < 0$ and $\lambda_2 = 0$. The method successfully captures the pressure minimum in a plane perpendicular to the vortex axis at high Reynolds numbers (Re), and accurately defines vortex cores at low Re, unlike a pressure minimum criterion.

TABLE II. Variation of separation and reattachment lengths L_1, L_2, and L_3, with channel aspect ratio A.

A	L_1 (roof / floor)	L_2 (roof / floor)	L_3 (roof / floor)
0.5	0.2060, 0.2059	0.2402, 0.2403	0.4107, 0.4154
0.6	0.2675, 0.2675	0.2434, 0.2435	0.4205, 0.4258
0.7	0.3152, 0.3153	0.2454, 0.2455	0.4206, 0.4264
0.8	0.3578, 0.3579	0.2467, 0.2468	0.4149, 0.4212
1.0	0.4277, 0.4279	0.2485, 0.2486	0.4007, 0.4068
1.2	0.4869, 0.4871	0.2494, 0.2495	0.3918, 0.3980
1.5	0.5506, 0.5510	0.2491, 0.2492	0.3873, 0.3936
1.7	0.5800, 0.5804	0.2480, 0.2481	0.3883, 0.3947
2.0	0.6138, 0.6143	0.2454, 0.2456	0.3933, 0.3997
2.5	0.6367, 0.6374	0.2387, 0.2388	0.4054, 0.4135
3.0	0.6272, 0.6280	0.2302, 0.2303	0.4201, 0.4293
4.0	0.5425, 0.5435	0.2097, 0.2099	0.4431, 0.4580
5.0	0.4410, 0.4422	0.1898, 0.1901	0.4572, 0.4835
6.0	0.3747, 0.3765	0.1745, 0.1750	0.4542, 0.5146
7.0	0.3361, 0.3388	0.1642, 0.1651	0.4255, 0.5620
8.0	0.3127, 0.3161	0.1577, 0.1584	0.4017, 0.5964
9.0	0.2969, 0.3000	0.1516, 0.1527	0.3910, 0.6190
10.0	0.2861, 0.2890	0.1477, 0.1486	0.3841, 0.6338
12.0	0.2719, 0.2749	0.1414, 0.1426	0.3753, 0.6535
15.0	0.2577, 0.2605	0.1357, 0.1366	0.3684, 0.6728
18.0	0.2499, 0.2525	0.1319, 0.1331	0.3654, 0.6839
24.0	0.2413, 0.2436	0.1268, 0.1278	0.3622, 0.6963
30.0	0.2369, 0.2391	0.1244, 0.1252	0.3606, 0.7030
36.0	0.2344, 0.2364	0.1231, 0.1238	0.3597, 0.7070
42.0	0.2328, 0.2349	0.1225, 0.1230	0.3592, 0.7095
48.0	0.2318, 0.2339	0.1217, 0.1226	0.3588, 0.7110
2-D	0.2296, 0.2323	0.1204, 0.1215	0.3583, 0.7136

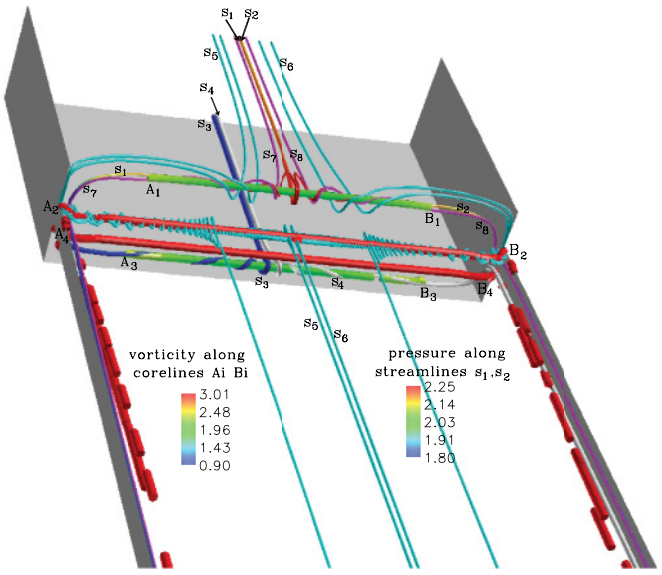

FIG. 6. (Color online) Extracted core lines A_1B_1/A_3B_3 and A_2B_2/A_4B_4 of the salient and tip eddies along the roof/floor. Spanwise opposite spatial evolution of (s_1,s_2), (s_3,s_4) reveals symmetry-plane flow bifurcates along the core lines A_1B_1 and A_3B_3 of the salient roof/floor eddies. 3D spatially converging growth of (s_5,s_6) surrounding A_2B_2 confirms no bifurcation occurs along the vortical core line of a tip eddy. $C = 4$, Re = 1500, and $A = 4$.

In Fig. 6, the thick lines A_1B_1/A_3B_3 are the spanwise extended core lines of the salient roof and floor eddies, and A_2B_2/A_4B_4 are the vortical core lines of the corresponding tip eddies [Fig. 3(a)(a)]. Notably, the downstream moving fluid particles, as evidenced by the physical dymanics (Fig. 6) of the streamlines (s_1,s_2), upon approaching the vortex core line A_1B_1, spiral along it in spanwise-opposite directions and gradually move away from the symmetry plane ($y = 0$). Note also that the fluid particles that originate from the left of s_1 (as exhibited by the streamline s_7) continue to roll toward the left (A_1), and those issuing from the right of s_2 (as revealed by s_8) continued to spiral toward the right (B_1) of the vortex core line A_1B_1. Therefore, the phenomenon of occurrence of symmetry-plane ($y = 0$) flow bifurcation over the core line A_1B_1 of the salient roof eddy remains well defined. Moreover, the spanwise opposite spiraling dynamics of the streamlines (s_3,s_4) surrounding A_3B_3 confirms the occurrence of a similar spanwise bifurcation of the symmetry-plane flow along the vortical core line A_3B_3 of the salient floor eddy. The present study thereby demonstrates the clear occurrence of local spanwise bifurcations of the developed 3D (steady) flow along the topological cores of the salient roof and floor eddies. As we will soon observe, such a bifurcation phenomenon occurs in plane 3D contraction channel flows virtually with all aspect ratios, suggesting that bifurcations are indeed not end-wall induced. In an effort to reveal the inner flow physics, in Fig. 6 we also extract pressure variation along the two near-symmetry-plane bifurcating streamlines (s_1,s_2) in the shedded form. It clearly shows the occurrence of a local pressure maximum at a spanwise bifurcation point over A_1B_1. On the other hand, it is indeed interesting to note that the gradually converging (inward) flow dynamics surrounding A_2B_2, as demonstrated by spatial evolution characteristics of the streamlines (s_5,s_6), reveals that no spanwise flow bifurcation surrounding the vortical core lines of the tip eddies takes place.

In order to strengthen our understanding of near-contraction flows, in Fig. 7(a) we extract symmetry-plane flow behavior (streamlines and u-velocity profiles) in a channel with a significantly lower contraction ratio $C = 2$ (and Re = 3150, $A = 7$). Notably, flow in the setup is now seen to evolve in a perfectly symmetric fashion. However, as the aspect ratio of the channel was gradually increased, the pitchfork bifurcation appeared again with its distinctive signature. To be precise, our simulated results with $A = 36$ [Fig. 7(b), also at $C = 2$, Re = 3150] reveal the occurrence of a notable relative enlargement of the downstream floor reattachment length (recirculation zone) compared to corresponding roof reattachment lengths, suggesting the clear existence of a pitchfork bifurcating solution beyond some critical aspect ratio. In contrary, a closer look at Figs. 7(a) and 7(b) reveals that a decrease in the aspect ratio has a stabilizing effect on the (downstream) flow. In an attempt to demonstrate consistency/stability, near-transitional flow behavior downstream of the three-dimensional sudden contraction has also been simulated with a significantly higher Reynolds number, Re = 3500 [while keeping $C = 2$ and $A = 36$ fixed, as in Fig. 7(b)], and such results are presented in Fig. 8(a). It clearly reveals a continued unequal inception of separation bubbles (tip eddies) along the roof and floor of the contraction zone owing to the persistence of pitchfork bifurcation. For the sake of clarity, topological growth of the

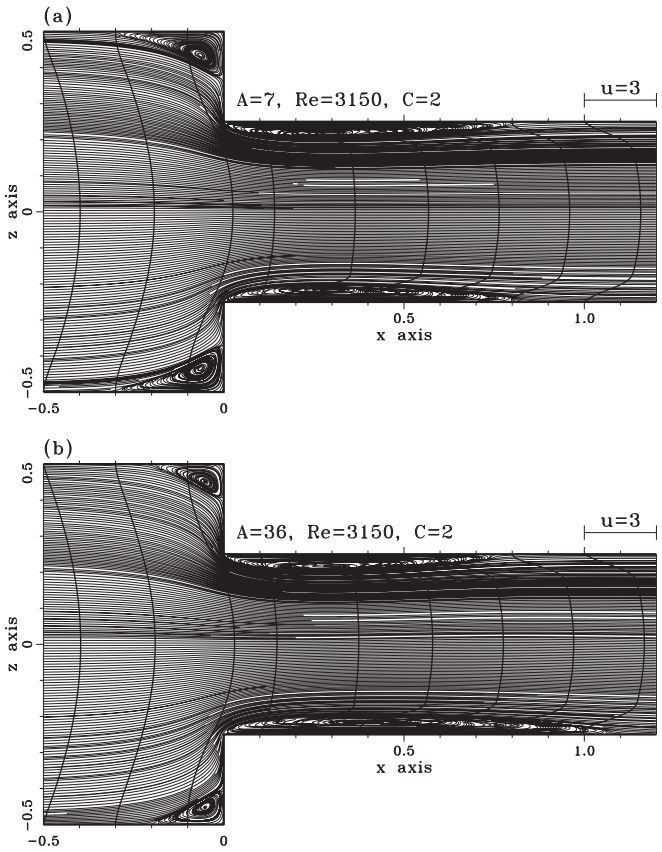

FIG. 7. Streamwise flow development in a contraction channel with $C = 2$. (a) Streamlines over the symmetry-plane ($y = 0$) and the extracted u-velocity profiles reveal nonbifurcating, perfectly symmetric flow development at $A = 7$. (b) Flow features at higher aspect ratio ($A = 36$) reveal dominance of pitchfork bifurcation within the contraction channel in the form of unequally grown tip eddies over the channel roof and floor.

near-side-wall flow through a pair of spiral nodes and a pair of saddles has been documented in Fig. 8(b). In addition, a detailed convergence history of such a flow is extracted in Fig. 8(c).

At this point, in an attempt to examine three-dimensional structural flow mechanisms, in Fig. 9 we extract the simulated vortical core lines of various floor and roof (salient/tip) eddies, and the surrounding important flow dynamics corresponding to $C = 2$, Re = 3150, and $A = 7$. Notably, spanwise opposite spiraling behavior of the streamlines (s_1,s_2) surrounding the core line A_1B_1 of the salient roof eddy reveals the occurrence of a spanwise bifurcation of the oncoming flow over A_1B_1. We mention here that a similar spanwise bifurcation of the symmetry-plane flow along the core line of the salient floor eddy has also been noted to occur (by virtue of the perfectly symmetrical growth of roof and floor salient eddies and the supporting physics). For the sake of enhanced clarity, the occurrence of a local pressure maximum at the bifurcation point over A_1B_1 has also been shown here (Fig. 9) with the help of extracted pressure values along s_1 and s_2. We would like to state at this point that a similar spanwise bifurcation phenomenon along vortical core lines of the salient (roof and floor) eddies has been noted to occur for all other higher aspect

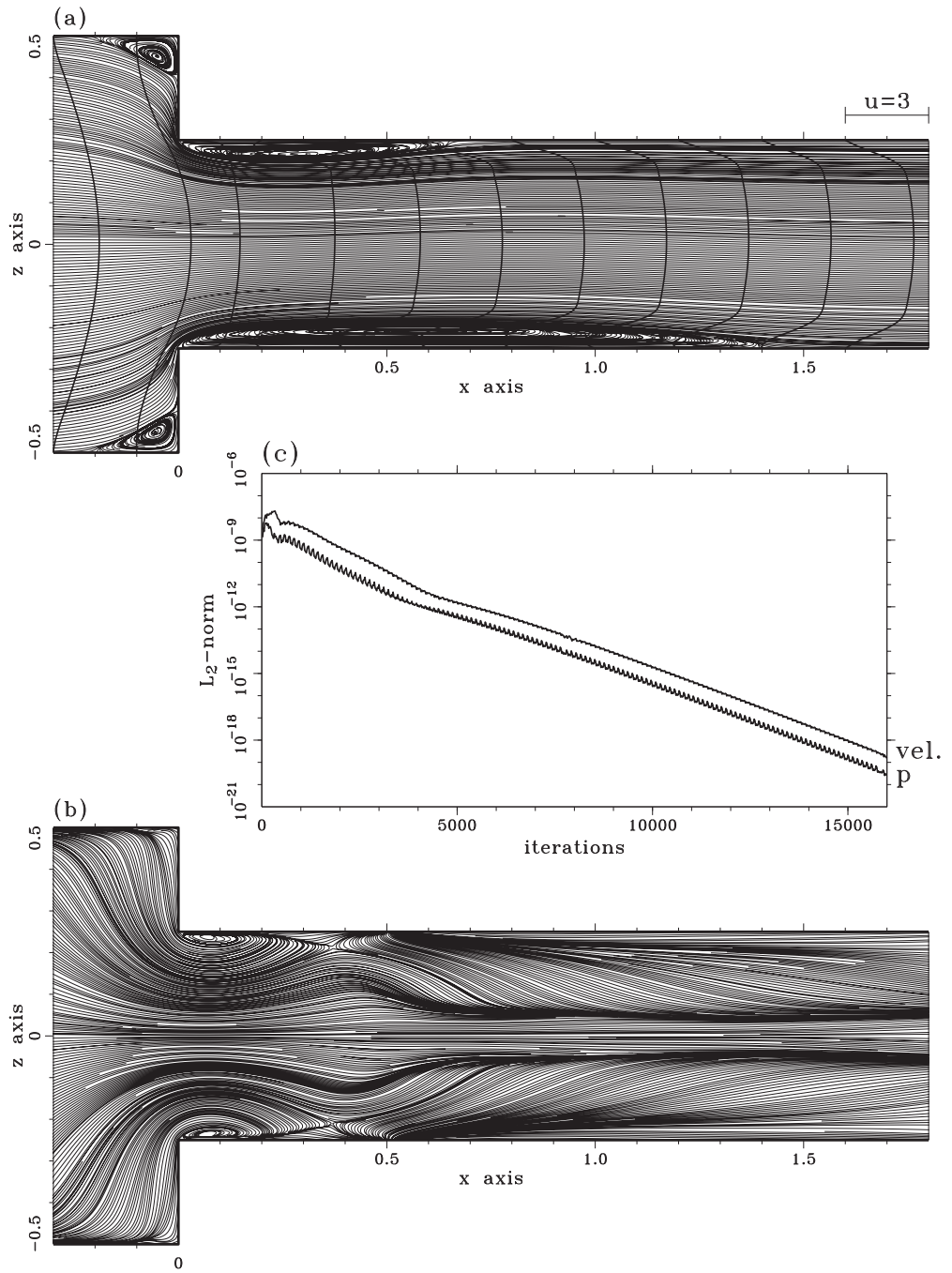

FIG. 8. Presence of a steady pitchfork bifurcating solution in a contraction channel at Re = 3500. (a) Streamlines over the symmetry plane ($y = 0$) reveal dominant bifurcating flow characteristics. (b) Limiting streamlines on the left sidewall. (c) L_2 norm of the convergence history. $A = 36$ and $C = 2$.

ratios (e.g., $A = 48$), however, their graphical representation becomes difficult due to the large value of A (channel span) with respect to the transverse width D. On the other hand, remarkably, the spatially converging spiral evolution (Fig. 9) of streamlines s_3 and s_4 surrounding the core line A_2B_2 [of the roof tip eddy, as noted in Fig. 7(a)] suggests that no spanwise flow bifurcation over the vortical core lines of the tip eddies takes place.

Figure 10 further unfolds the internal flow physics across two important transverse sectional planes ($x = -0.05$ and $x = 0.25$) passing through the salient and tip eddies [Fig. 7(a)]. Notably, pressure contours on $x = -0.05$ [Fig. 10(a)] reveal symmetrical growth of two distinct relative high-pressure regions extending along the roof and floor of the expansion zone. In particular, note that the presence of a relative local high-pressure zone [Fig. 10(a)] on the roof surrounding $(y,z) = (0.0,0.5)$ is clearly reflected in Fig. 9 by virtue of the demonstrated occurrence of pressure maximum at the bifurcation point over A_1B_1. On the other hand, note the development of a core low-pressure region spanning over $z = 0$ [Fig. 10(a)].

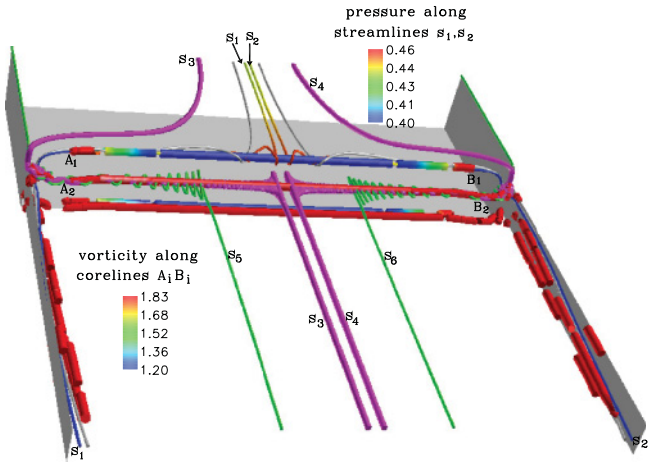

FIG. 9. (Color online) Symmetry-plane spanwise bifurcation at $C = 2$, Re $= 3150$, and $A = 7$. Spanwise opposite spatial evolution of (s_1,s_2) shows symmetry-plane flow bifurcates along the core line A_1B_1 of the salient roof eddy. Spatial growth of (s_3,s_4) surrounding A_2B_2 confirms that no flow bifurcation occurs along the core line of the tip eddy.

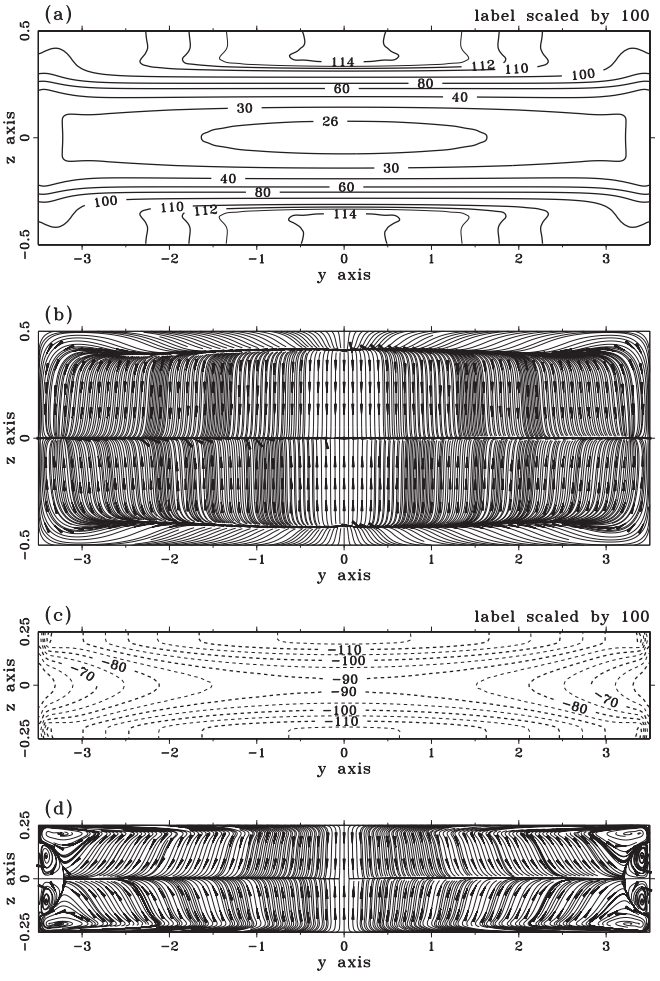

FIG. 10. Pressure contours and cross-stream flow behavior through different transverse sections. (a) Pressure contour on $x = -0.05$, (b) streamlines on $x = -0.05$, (c) pressure contour on $x = 0.25$, and (d) streamlines on $x = 0.25$. $C = 2$, Re $= 3150$, and $A = 7$.

Interestingly, the stretching behavior of streamlines on $x = -0.05$ clearly demonstrates the physically realistic fact that the fluid (over the yz plane) gets accelerated from (roof and floor) high-pressure zones to the (central) low-pressure zone (a fact widely demonstrated in some of our recent works, e.g., Refs. [12,23]). Note that the near-roof and near-floor oppositely stretching dynamics [Fig. 10(b)] of the streamlines is caused due to dominant locally recirculating 3D flow surrounding two core lines of the salient (roof and floor) eddies. Figures 10(c) and 10(d) exhibit the pressure distribution and the associated streamline behavior, respectively, on a sectional plane $x = 0.25$, which passes through the downstream (roof and floor) tip eddies. In Figs. 10(c)–10(d), the scale along the z axis is magnified by a factor 2.4 in order to have a closer look at the local physical flow characteristics. Notably, while the

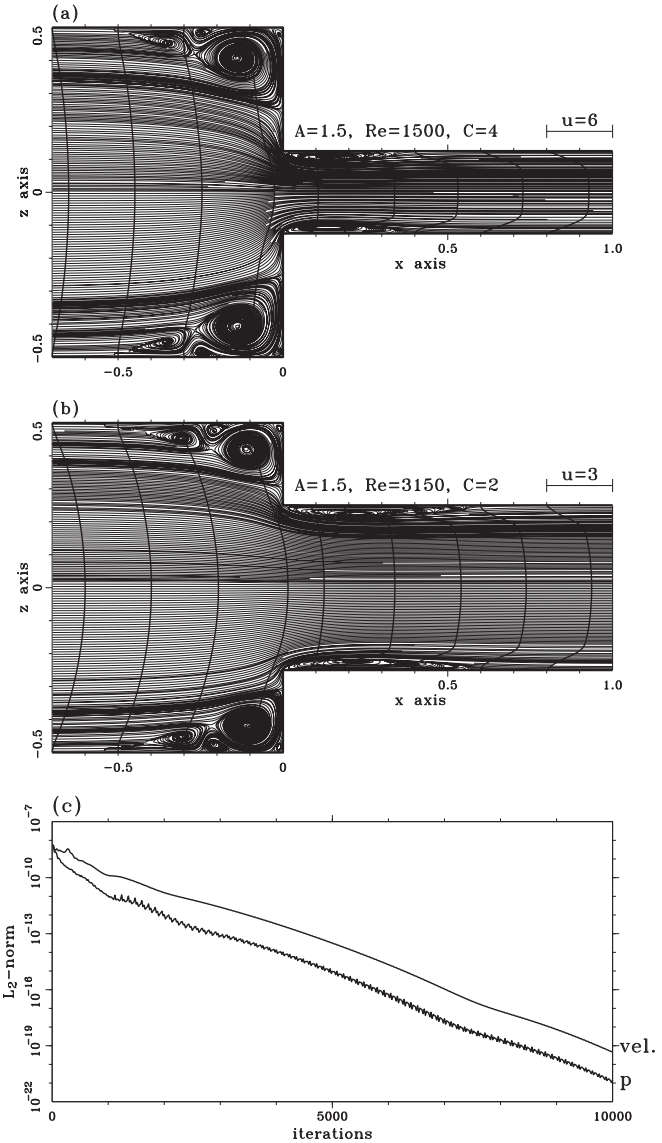

FIG. 11. Physically important splitting of salient eddies with low aspect-ratio ($A = 1.5$) channels. (a) Streamlines (on $y = 0$) and u-velocity profiles (at $C = 4$) reveal axial-symmetric flow development with fractured salient roof/floor eddies; (b) symmetry-plane flow evolution at $C = 2$; and (c) L_2 norm of the convergence history at $A = 1.5$, $C = 2$, and Re $= 3150$.

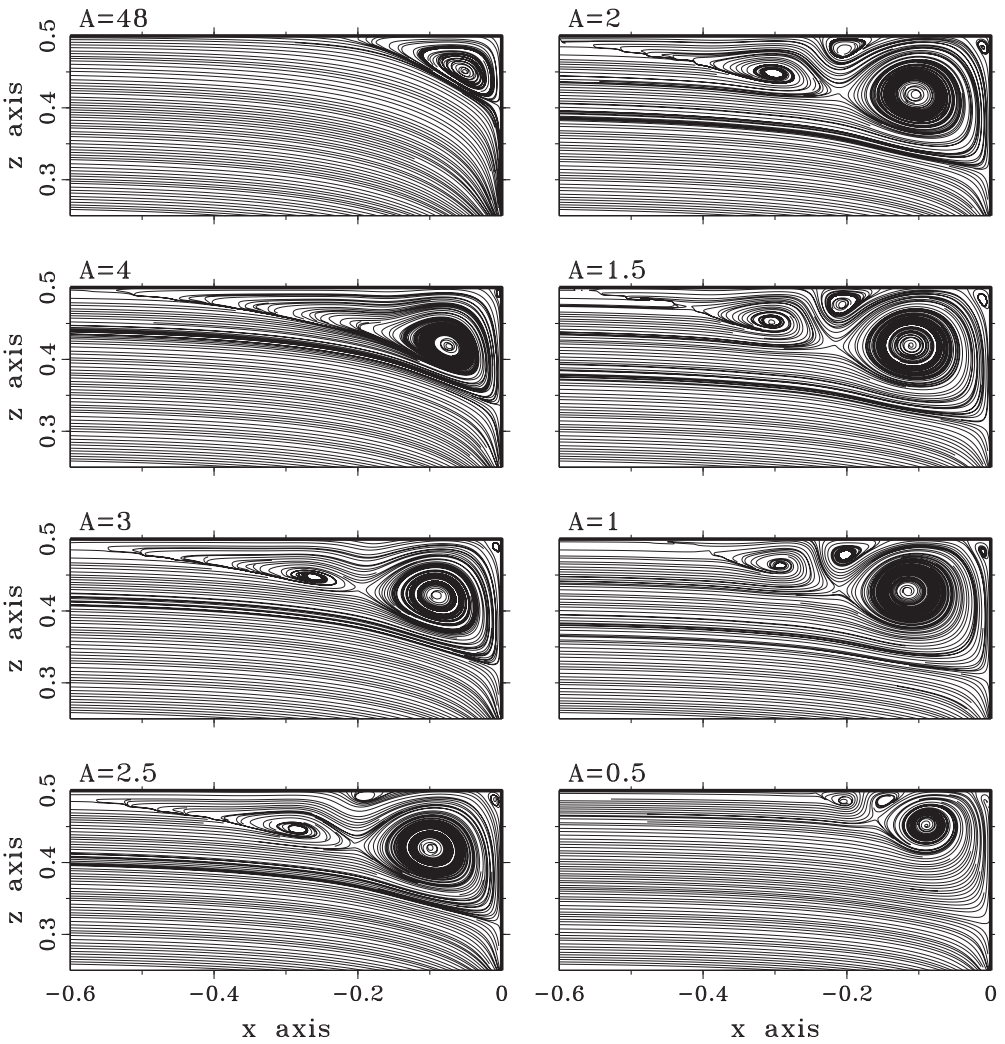

FIG. 12. Aspect-ratio-dependent structural evolution of a salient eddy with $C = 2$ and Re = 3150.

vortical structures at four corners [Fig. 10(d)] correspond to the presence of corner eddies [24] in the setup, the other two pairs of relatively smaller symmetrical recirculations observed at the spanwise ends (of the $z = 0$ line) seem to identify downstream extension of the near-wall snecked eddies, as noted in Fig. 9. On the other hand, once again, the depicted pressure contours [Fig. 10(c)] on $x = 0.25$ in association with corresponding sectional flow [Fig. 10(d)] patterns seem to confirm the realistic fact that fluid gets accelerated from a high-pressure magnitude zone toward a neighboring low-pressure zone.

We now examine physical flow development in a significantly low aspect-ratio channel. For this, Fig. 11(a) first captures the symmetry-plane flow details at $A = 1.5$, Re = 1500, and $C = 4$. The corresponding flow features with a moderate aspect-ratio channel (with $A = 4$, Re = 1500, and $C = 4$) have been described in Fig. 3(a). Interestingly, unlike with moderate/high aspect-ratio channels ($4 \leqslant A \leqslant 48$), as noted in Figs. 3, 4, 7, and 8, the upstream salient roof and floor eddies (at $A = 1.5$) are now seen to decompose into three smaller constituents both at $C = 4$ [Fig. 11(a)] and $C = 2$ [Fig. 11(b)]. On the other hand, remarkably, the downstream flows show no sign of asymmetry/pitchfork bifurcation (note in this context the very symmetrical growth of the u-velocity profiles). A similar fractured structural growth of salient eddies has also been observed for a further lower aspect-ratio ($A = 0.5$) channel. Figure 11(b) reconfirms a very consistent splitting behavior of the salient roof and floor eddies with Re = 3150, $C = 2$, and $A = 1.5$. Corresponding flow characteristics with a moderate aspect-ratio channel (e.g., with $A = 7$, Re = 3150, and $C = 2$) have been extracted in Fig. 7(a). Note that the observed physical splitting [Figs.11(a) and 11(b)] of upstream salient (roof and floor) eddies into multiple (two or three) smaller constituents is an inherent feature of the low aspect-ratio flows. For the sake of completeness, in Fig. 11(c) we demonstrate the convergence characteristics of such a flow in terms of the computed L_2-error norm. For a broader understanding, Fig. 12 summarizes the aspect-ratio-dependent structural evolution of a salient roof eddy over the symmetry plane $y = 0$ (the corresponding salient floor eddy also evolves exactly in the same manner as the roof eddy). To be explicit, Fig. 12 clearly exhibits the triple vortex type structural growth of the salient eddy within $0.5 \leqslant A \leqslant 2.0$. It takes a double vortex form within $2.75 \leqslant A \leqslant 3.5$ before eventually attaining the single vortex type evolution phase with $A \geqslant 4$. We will

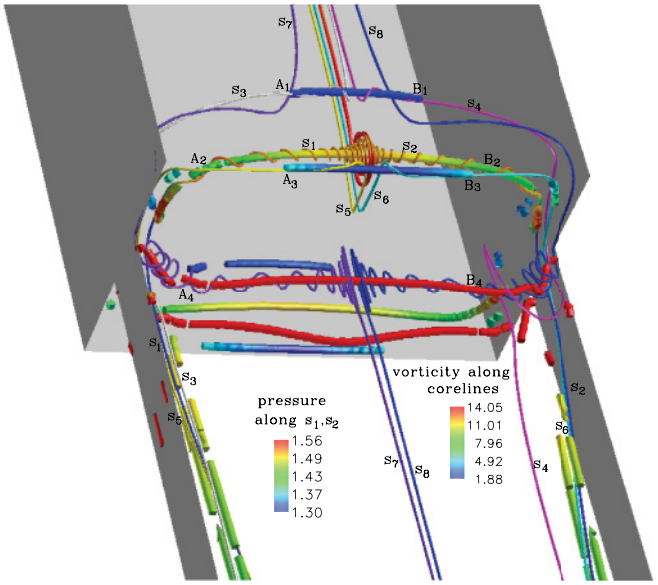

FIG. 13. (Color online) Symmetry-plane spanwise flow bifurcation in a small aspect-ratio channel. Spanwise oppositely spiraling evolution of (s_3,s_4), (s_1,s_2), and (s_5,s_6) shows symmetry-plane flow bifurcates along each of the core lines A_1B_1, A_2B_2, and A_3B_3 of a fractured salient roof eddy. Inward converging 3D spiral growth of (s_7,s_8) surrounding A_4B_4 shows that no flow bifurcation occurs along the vortical core line of the tip eddy. $A = 1.5$, $C = 4$, and Re $= 2000$.

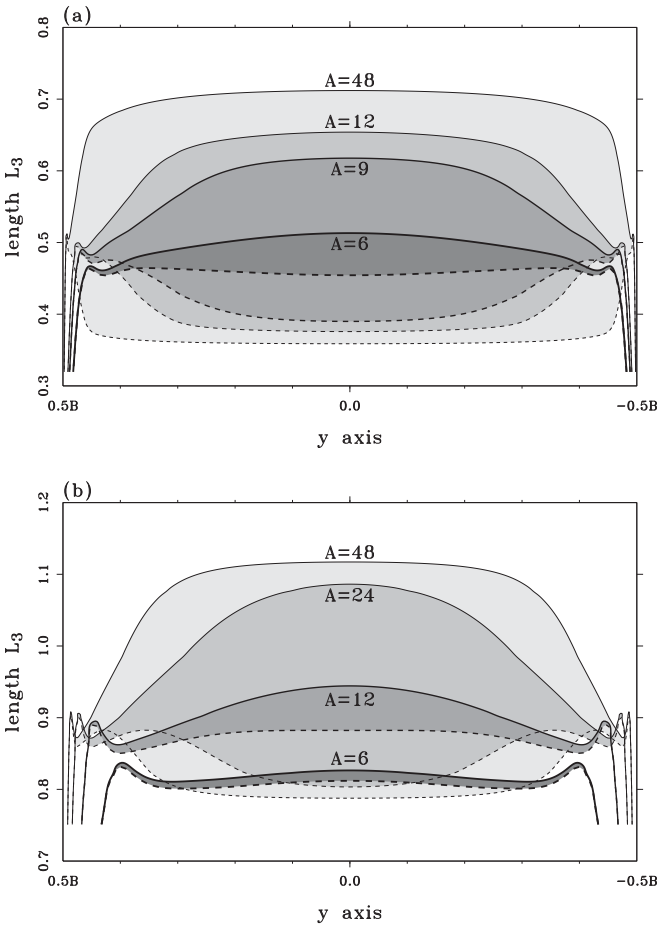

FIG. 14. Spanwise-streamwise variations of reattachment length L_3 over the roof (dotted lines) and floor (solid lines) with different aspect ratios exhibit the onset of pitchfork type flow bifurcation. (a) $C = 2$ and Re $= 3150$. (b) $C = 4$ and Re $= 1500$.

soon discover that the corresponding spanwise flows undergo symmetry-plane $(y = 0)$ bifurcation along the topological core lines of each of these fractured salient roof and floor eddies. In this context, readers may, however, note the persistence of single-core structural evolution of the salient eddy for semidilute polymer flows through an 8:1 contraction-ratio planner microchannel [25].

Figure 13 demonstrates the complex near-contraction three-dimensional structural features of a small aspect-ratio $(A = 1.5)$ channel flow in which multiple symmetry-plane bifurcations occur along the vortical core lines of the fractured salient eddies. The thick lines A_1B_1, A_2B_2, and A_3B_3 in Fig. 13 represent the simulated vortical core lines of the three fractured salient roof eddies. Notably, the oppositely spiraling dynamics of streamlines (s_3,s_4), (s_1,s_2), and (s_5,s_6) along A_1B_1, A_2B_2, and A_3B_3, respectively, confirms the occurrence of three simultaneous local spanwise flow bifurcations (in the vicinity of $y = 0$) over the topological core lines of the (fractured) salient roof eddies. For the sake of enhanced clarity, the clear occurrence of local pressure maximum at the bifurcation point on A_2B_2 has also been confirmed here with the help of extracted pressure magnitudes along s_1 and s_2. We may mention here that similar upstream spanwise triple bifurcations (over the symmetry plane $y = 0$) are also observed to occur along the vortical core lines of the corresponding (fractured) salient floor eddies. However, for the sake of maintaining cleanliness, those are not extracted in Fig. 13. On the other hand, quite remarkably, the inward spiraling dynamics of the streamlines (s_7,s_8) surrounding the core line A_4B_4 (of the roof tip eddy) shows that there takes place no flow bifurcation along the vortical core line of a tip eddy. Note also in Fig. 13 the variation of vorticity magnitude along A_2B_2. Vorticity appears to attain local maximum at the symmetry-plane $(y = 0)$ bifurcation point.

At this point, it may be appropriate to address the issue of possible coupling between the downstream pitchfork bifurcation (Figs. 4 and 8) and the upstream spanwise bifurcations (Figs. 6 and 13) observed over the symmetry plane $y = 0$. It is important to note here that for the investigated moderate range of Re, the (bifurcated) flows remained stable/steady. Such a steady character of the flow enforces a near-linear/smooth variation of the downstream attachment lengths (L_3) over the major span of the channel [e.g., Fig. 14(a)], except near the close vicinity of sidewalls, where viscous force dominates. Moreover, at this moderate Re (steady regime) the formation of a single symmetry-plane spanwise flow bifurcation over a core line of an upstream salient eddy, owing to the occurrence of a corresponding single-point pressure maximum over the eddy core lines (while maintaining spanwise symmetry) is noted. Once Re is slowly increased to (unsteady) near-transitional states, these core lines of the salient eddies will start behaving like vibrating strings (with pressure/velocity oscillating along the spanwise extended core lines), initially with appearances of equidistant multiple pressure maxima and the corresponding uniformly spaced spanwise bifurcation points (over the core lines). As a consequence, we expect to encounter wavy growth

of L_3 over the channel span. At a near-turbulent state, the uniform length-scaled bifurcations (over the upstream salient eddy core lines) are expected to be replaced by random occurrences of bifurcation points and associated arbitrary spatiotemporal growth of local pressure maxima along the core lines of the salient eddies, leading to the formation of coherent-like structures on the channel roof and floor. A systematic study describing exactly how spanwise bifurcations evolve in the case of transitional bluff body wakes has been documented in some of our recent works [21,26]. On the other hand, concerning the issue of stability of the contraction flow (and a source of potential future investigation), the theoretical method as proposed by Scarsoglio *et al.* [27] and Scarsoglio and Tordella [28] may be suitably implemented to study detailed bifurcation characteristics in the setup. However, this appears to be beyond the scope of present investigation.

In order to provide a quantitative analysis concerning global variation of $L_3(x,y)$, in Fig. 14(a) we extract distributions of $L_{3,\text{roof}}$ (solid lines) and $L_{3,\text{floor}}$ (corresponding dotted lines in a loop) for some of the selected aspect ratios (by keeping $C = 4$ and $\text{Re} = 3150$ fixed). Notably, while the distributions of both $L_{3,\text{roof}}$ and $L_{3,\text{floor}}$ (for the roof and floor tip eddies) mostly remained flat over the major part of the channel span (except in close vicinity of the sidewalls), their streamwise gap (the projected difference, $L_{3,\text{roof}} - L_{3,\text{floor}}$) continued to decrease with the reduction of channel aspect ratio, clearly suggesting that there remains a critical aspect ratio which facilitates the onset of downstream pitchfork bifurcation. For the sake of broader understanding, variations of $L_{3,\text{roof}}$ and $L_{3,\text{floor}}$ (with A) for contraction flows corresponding to $(C, \text{Re}) = (4, 1500)$ have been extracted in Fig. 14(b). Importantly, however, both Figs. 14(a) and 14(b) seem to suggest that the reduction in the channel aspect ratio (spanwise width) facilitates stabilization of the downstream flow (as the projected gap between $L_{3,\text{roof}}$ and $L_{3,\text{floor}}$; that is, asymmetry continues to reduce steadily with decreasing A).

Figure 15 provides an explicit mapping for variations of different separation/reattachment lengths L_1, L_2, and L_3 (of salient and tip eddies) with aspect ratio A. Importantly, the separation length L_1 (of salient eddies) continues to increase exponentially [Fig. 15(a)] for small aspect-ratio channels having $A \leqslant 2.5$; subsequently, steep streamwise reduction (of L_1) of the separation bubbles occurs (for the moderate aspect-ratio channels) within the parameter space $3 \leqslant A \leqslant 8$, before eventually asymptotically attaining the two-dimensional reference value in the range $A \geqslant 25$. Notably, the aspect ratio A seems to have little bearing [Fig. 15(a)] on the attachment length L_2. On the other hand, interestingly, the reattachment lengths L_3 (of the tip eddies) over the channel roof and floor are seen [Fig. 15(b)] to vary equally (exhibiting continuation of the nonbifurcating flow regime) up to $A \leqslant 5$, then their difference $(L_{3,\text{roof}} - L_{3,\text{floor}})$ continues to grow steadily (facilitating the onset and persistence [EDG1] of pitchfork bifurcation in the setup) with increasing aspect ratio, before eventually reaching an asymptotic state (coinciding with the two-dimensional reference value) for $A \geqslant 40$. Note that a similar aspect-ratio dependence of the separation/reattachment lengths L_1, L_2, and L_3 of salient and tip eddies in contraction channels with contraction ratio $C = 4$ has been found to persist, and such results are graphically presented in Figs. 16(a)–16(b).

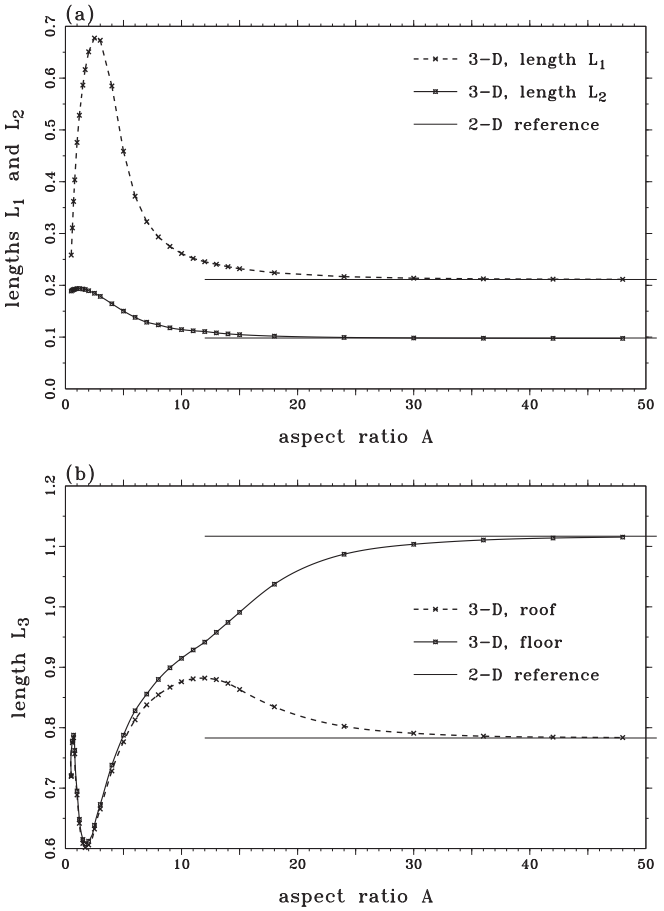

FIG. 15. Variations of symmetry-plane separation/reattachment lengths L_1, L_2, and L_3 with aspect ratio A. (a) Dependence of L_1 and L_2 on A; $C = 2$ and $\text{Re} = 3150$. Large aspect-ratio values are seen to asymptotically converge to the corresponding 2D reference solution. (b) Variations of reattachment lengths L_3 over the channel roof/floor with respect to A. $C = 2$ and $\text{Re} = 3150$.

It is important to note, however, that the persisting difference of $L_{3,\text{roof}}$ and $L_{3,\text{floor}}$ values of the corresponding roof and floor (tip) eddies for $A \geqslant 5$ [Figs. 15(b) or 16(b)] are obtained based on a fixed Reynolds number, and we strongly feel a contraction channel will continue to exhibit pitchfork/spanwise bifurcating solutions irrespective of the spanwise extent A of the channel (however small/large A may be), or its contraction ratio C, once Re is increased sufficiently. The value of critical Re in a setup, however, will depend on its aspect ratio (A) and the contraction ratio (C). In other words, our findings strongly suggest that the onset of flow transition in a sudden contraction channel should inevitably occur through the presently documented pitchfork and spanwise bifurcation modes.

IV. CONCLUSIONS

Within the framework of the present study we have computationally revealed the important physical characteristics of steady state flows in the vicinity of a three-dimensional sudden contraction. While being consistent with the known symmetry-plane solutions/measurements, the present 3D simulations help to significantly enhance our knowledge on the issue of

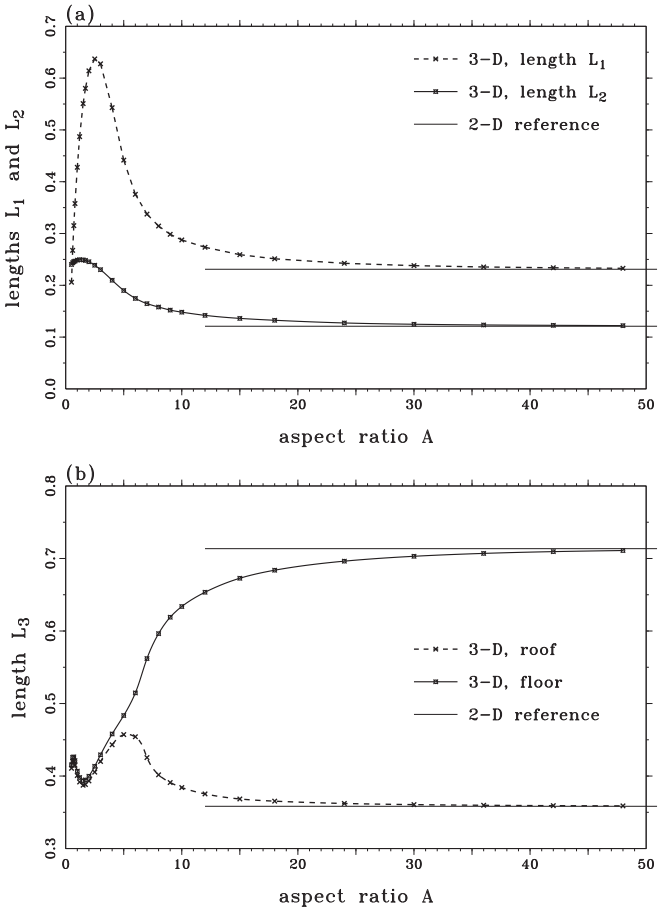

FIG. 16. Dependence of separation/reattachment lengths L_1, L_2, and L_3 of salient/tip eddies on aspect ratio A. (a) Variations of L_1 and L_2 with A; $C = 4$ and $\mathrm{Re} = 1500$. Large aspect-ratio values are seen to asymptotically converge to the corresponding 2D reference solutions. (b) Symmetry-plane variations of reattachment lengths L_3 over the channel roof and channel floor with respect to A. $C = 4$ and $\mathrm{Re} = 1500$.

growth of asymmetric/bifurcating solutions in the physical setup.

Physically, on the issue of entrainment in the upstream region, the dominant salient (roof and floor) eddies are seen to facilitate pumping out the oncoming near-symmetry-plane fluid towards the channel sidewalls, whereas the downstream tip eddies continued to effectively entrain the near-wall outer fluid into the core of the contraction channel. In the process, the upstream symmetry-plane flow is noted to get bifurcated along the vortical core lines of each of the salient roof and floor eddies, and much of the outer fluid moved inward along the cores of tip corner eddies. Concerning the governing physics, in the upstream, the streamwise extended localized growth of relative high-pressure regions along the channel roof and floor (while their cores remain aligned with the vertical plane of symmetry) and development of a low-pressure region spanning all along the horizontal symmetry plane seem to facilitate the physical mechanism of growth of the near-contraction flow. As the channel aspect ratio was reduced considerably, we observed interesting splitting (fractured growth) of both the salient roof and floor eddies in the form of triplets, and the oncoming (vertical) symmetry-plane flow continued to bifurcate along the spanwise extended vortical core lines of each of these split salient eddies.

In contrary, once the channel aspect ratio was gradually increased (beyond some critical value), we noted the onset/occurrence of symmetry-breaking pitchfork bifurcation of the flow downstream of sudden contraction. Unequal growths of tip-corner separation bubbles (tip eddies) and their reattachment lengths along the roof and the floor of the contraction zone confirm the occurrence of such a pitchfork bifurcation in the symmetrical setup. Importantly, the observed sustainable presence (persistence) of these spanwise/pitchfork bifurcation modes both at higher Re and higher aspect ratios suggests such bifurcations are indeed inherent critical features of three-dimensional sudden-contraction flows, and possibly indicate logical paths leading to eventual flow transition.

[1] D. V. Boger, Ann. Rev. Fluid Mech. **19**, 157 (1987).
[2] S. C. R. Dennis and F. T. Smith, Proc. R. Soc. London, Ser. A **372**, 393 (1980).
[3] F. Durst and T. Loy, Comput. Fluids **13**, 15 (1985).
[4] F. Durst, W. F. Schierholz, and A. M. Wunderlich, ASME J. Fluids Eng. **109**, 376 (1987).
[5] D. M. Hawken, P. Townsend, and M. F. Webster, Comput. Fluids **20**, 59 (1991).
[6] H. Huang and B. R. Seymour, Comput. Fluids **24**, 153 (1995).
[7] F. Durst, A. Melling, and J. H. Whitelaw, J. Fluid Mech. **64**, 111 (1974).
[8] W. Cherdron, F. Durst, and J. H. Whitelaw, J. Fluid Mech. **84**, 13 (1978).
[9] R. M. Fearn, T. Mullin, and K. A. Cliffe, J. Fluid Mech. **211**, 595 (1990).
[10] J. Mizushima, H. Okamoto, and H. Yamaguchi, Phys. Fluids **8**, 2933 (1996).
[11] J. Mizushima and Y. Shiotani, J. Fluid Mech. **434**, 355 (2001).
[12] A. Sau, Phys. Fluids **14**, 3280 (2002).
[13] A. Sau, T. W. H. Sheu, R. R. Hwang, and W. C. Yang, Phys. Rev. E **69**, 066302 (2004).
[14] B. P. Leonard, Comput. Methods Appl. Mech. Eng. **19**, 59 (1979).
[15] T. P. Chiang, R. R. Hwang, and T. W. H. Sheu, Int. J. Numer. Meth. Fluids **23**, 325 (1996).
[16] J. P. Van Doormaal and G. D. Raithby, Numer. Heat Transfer **7**, 147 (1984).
[17] R. Hunt, J. Numer. Methods Fluids **11**, 247 (1990).
[18] J. Mizushima and Y. Shiotani, J. Fluid Mech. **420**, 131 (2001).
[19] T. P. Chiang and T. W. H. Sheu, Trans. ASME, J. Fluid Eng. **124**, 444 (2002).
[20] T. P. Chiang, T. W. Sheu, R. Hwang, and A. Sau, Phys. Rev. E **65**, 016306 (2002).

[21] A. Sau, Phys. Fluids **21**, 034105 (2009).
[22] J. Jeong and F. Hussain, J. Fluid Mech. **285**, 69 (1995).
[23] A. Sau, Phys. Rev. E **69**, 056307 (2004).
[24] H. K. Moffatt, J. Fluid Mech. **18**, 1 (1964).
[25] S. C. Omowunmi and X. F. Yuan, Rheol. Acta **49**, 585 (2010).
[26] A. Sau, Phys. Fluids **20**, 104108 (2008).
[27] S. Scarsoglio, D. Tordella, and W. O. Criminale, Stud. Appl. Math. **123**, 153 (2009).
[28] S. Scarsoglio and D. Tordella, Phys. Rev. E **81**, 036326 (2010).